

RhoB upregulation leads to either apoptosis or cytostasis through differential target selection

Laura A Marlow¹, Ilah Bok¹, Robert C Smallridge^{1,2,3} and John A Copland^{1,3}

Departments of ¹Cancer Biology, ²Internal Medicine, Division of Endocrinology, and ³Endocrine Malignancy Working Group, Mayo Clinic, 4500 San Pablo Road, Jacksonville, Florida 32224, USA

Correspondence should be addressed to J A Copland
Email
copland.john@mayo.edu

Abstract

Anaplastic thyroid carcinoma is a highly aggressive undifferentiated carcinoma with a mortality rate near 100% due to an assortment of genomic abnormalities which impede the success of therapeutic options. Our laboratory has previously identified that *RhoB* upregulation serves as a novel molecular therapeutic target and agents upregulating *RhoB* combined with paclitaxel lead to antitumor synergy. Knowing that histone deacetylase 1 (HDAC1) transcriptionally suppresses *RhoB*, we sought to extend our findings to other HDACs and to identify the HDAC inhibitor (HDACi) that optimally synergize with paclitaxel. Here we identify HDAC6 as a newly discovered *RhoB* repressor. By using isoform selective HDAC inhibitors (HDACi) and shRNAs, we show that *RhoB* has divergent downstream signaling partners, which are dependent on the HDAC isoform that is inhibited. When *RhoB* upregulates only p21 (cyclin kinase inhibitor) using a class I HDACi (romidepsin), cells undergo cytostasis. When *RhoB* upregulates BIM_{EL} using class II(I) HDACi (belinostat or vorinostat), apoptosis occurs. Combinatorial synergy with paclitaxel is dependent upon *RhoB* and BIM_{EL} while upregulation of *RhoB* and only p21 blocks synergy. This bifurcated regulation of the cell cycle by *RhoB* is novel and silencing either p21 or BIM_{EL} turns the previously silenced pathway on, leading to phenotypic reversal. This study intimates that the combination of belinostat/vorinostat with paclitaxel may prove to be an effective therapeutic strategy via the novel observation that class II(I) HDACi antagonize HDAC6-mediated suppression of *RhoB* and subsequent BIM_{EL}, thereby promoting antitumor synergy. These overall observations may provide a mechanistic understanding of optimal therapeutic response.

Key Words

- ▶ anaplastic thyroid carcinoma
- ▶ HDAC
- ▶ RhoB
- ▶ BIM
- ▶ p21

Endocrine-Related Cancer
(2015) 22, 777–792

Introduction

No effective therapy or standard of care exists for anaplastic thyroid carcinoma (ATC) patients since it is a rapidly progressing cancer with median survival of 3–5 months with near 100% fatality (Smallridge et al. 2009). These patients desperately needed new interventional therapy to manage this malignant disease. Using genomic profiling,

we previously detailed a novel signaling pathway where RhoB in combination with the microtubule stabilizer, paclitaxel, had antitumor synergy in ATC (Marlow et al. 2009). An intriguing preclinical finding was that a novel peroxisome proliferator activated receptor gamma (PPAR γ) agonist, efatutazone (aka CS-7017, RS5444), induced RhoB

expression causing an upregulation of the cyclin kinase inhibitor gene (*CDKN1A*) and its p21^{WAF1/CIP1} (p21) protein. p21 was necessary for inhibition of cell proliferation via G0/G1 cell cycle arrest and by silencing *PPAR γ* , *RhoB*, or *p21* we showed that the growth inhibitory effects of efatutazone was nullified (Marlow *et al.* 2009). Thus, we identified a sequential pathway in which efatutazone-*PPAR γ* -*RhoB*-p21 cell cycle arrest. In addition, we found that paclitaxel in combination with efatutazone possessed strong proapoptotic cell death synergy, doubling the apoptotic effects of paclitaxel (Marlow *et al.* 2009). These *in vitro* and *in vivo* preclinical discoveries led to a phase 1 clinical trial in ATC patients combining efatutazone with paclitaxel for which we have recently reported encouraging results (Smallridge *et al.* 2013). A multisite national phase 2 clinical trial was opened in September 2014. Here we further examine the role of *RhoB* in ATC. *RhoB* is a member of the Ras superfamily of isoprenylated small GTPases which unlike oncogenic RhoA and RhoC, possesses antitumor activity (Prendergast 2001a). Depending upon its cellular localization, *RhoB* exerted different functions. In the cytoplasm, it regulated actin organization and vesicle transport. *RhoB* was suppressed but not mutated in numerous cancers that include head and neck, colon, and lung cancers (Adnane *et al.* 2002, Agarwal *et al.* 2002, Mazieres *et al.* 2004). Multiple stimuli upregulated or suppressed *RhoB* including stress and growth stimuli (Fritz & Kaina 2001, Ader *et al.* 2002, Jiang *et al.* 2003, 2004, Ishida *et al.* 2004). Multiple therapeutics have been discovered to upregulate *RhoB* and were associated with antitumor activity. These include farnesyl transferase inhibitors, HDAC inhibitors (HDACi), hydroxymethylglutaryl-CoA reductase inhibitor (statins), and glucocorticoids (Prendergast 2001b, Agarwal *et al.* 2002, Allal *et al.* 2002, Furumai *et al.* 2002, Chen, *et al.* 2006, Marlow *et al.* 2010). *RhoB* activity has been shown to cause apoptosis in transformed cells (Prendergast 2001a). However, we found that efatutazone induced *RhoB* mediated cell cycle arrest and not apoptosis (Copland *et al.* 2006, Marlow *et al.* 2009). To seek a more powerful therapeutic than efatutazone plus paclitaxel and to better understand *RhoB* mechanism(s) of action, we reasoned to use HDACi plus paclitaxel, since previous studies showed that the use of a class I/II HDACi led to apoptosis (Mitsiades *et al.* 2005, Catalano *et al.* 2007, Borbone *et al.* 2010, Chan *et al.* 2013). Additionally, histone deacetylase 1 (HDAC1) can directly suppress *RhoB* mRNA via binding to an inverted CCAAT box in the *RhoB* promoter (Wang *et al.* 2003). We hypothesized that by re-expressing *RhoB*, HDACi leads to apoptosis and antitumor synergy when combined

with paclitaxel for improved patient prognosis. HDACi modulate acetylation by targeting histone deacetylases and serve as powerful antitumor agents since they induce differentiation and apoptosis via transcriptional modulation. To date, a Class I HDACi, romidepsin (depsipeptide/FK228) and a Class II/(I) HDACi, vorinostat (SAHA/MK-0683), were FDA approved for treating cutaneous T-cell lymphoma (Nebbio *et al.* 2009, Prince *et al.* 2009, New *et al.* 2012). Another class II/(I) HDACi, belinostat (PXD101) was FDA approved for relapsed or refractory peripheral T-cell lymphoma (Lee *et al.* 2015) and panobinostat (LBH589) was recently approved for multiple myeloma ([no authors] 2015). Other HDACi are currently in phase II clinical trials including: givinostat (ITF2357), mocetinostat (MGCD0103), quisinostat (JNJ-26481585), pracinostat (SB939), resminostat (4SC-201), entinostat (MS-275), abrexinostat (PCI-24781), and valproic acid as a HDACi (previously FDA approved for epilepsy). Class I HDACs encompassed HDAC1-3 and 8 while Class II, included HDAC4-7, 9 and 10 (Bertos *et al.* 2001, Zhou *et al.* 2001). Class III, also known as the silent information regulator 2 (Sir2) family, consisted of seven genes related to yeast Sir2, and possess nicotinamide-adenine dinucleotide (NAD⁺)-dependent deacetylase activity (Vaziri *et al.* 2001). Class IV have characteristics of both class I and class II HDACs with HDAC11 being its only member (Gao *et al.* 2002). Our current investigation used clinically relevant HDACi to delineate *RhoB*-mediated signaling pathways which bifurcate depending upon the class of HDACi used. When a class I HDACi led only to p21 upregulation and G0/G1 cell cycle arrest, then no synergy with a cytotoxic agent occurred. The upregulation of BIM_{EL} and G2/M arrest in ATC cell lines led to induction of apoptosis and antitumor synergy with cytotoxic therapy. For the first time, we described that HDAC6 transcriptionally suppressed *RhoB* to mediate the pro-apoptotic effects of class II/(I) HDACi. Both HDAC1 and HDAC6 upregulated *RhoB*, *CDKN1A* and *BIM* mRNA and thus, the absence of p21 or BIM protein expression after HDACi treatment was regulated via proteasome protein degradation mechanisms. We further demonstrated that HDAC1 and HDAC6 protein levels were elevated in ATC patient tissues indicative of potential therapeutic relevance.

Materials and methods

Reagents

The HDACi, belinostat (PXD101) and vorinostat (SAHA/MK-0683) and romidepsin (depsipeptide/FK-228)

were purchased from Selleck (Houston, TX, USA). Paclitaxel, MG132 and DMSO solvent were purchased from Sigma–Aldrich.

Cell culture

THJ-11T (*KRAS*, *TP53*, *TERT*), THJ-16T (*PI3KCA*, *TP53*, *TERT*), THJ-21T (*BRAF*, *TP53*, *TERT*) and THJ-29T (*APC*, *TP53*, *TERT*) ATC cell lines were originated in our laboratory (Marlow *et al.* 2010) and were short-tandem repeat verified and validated to the respective patient's ATC tissue. The *APC* mutation for THJ-29T was identified by Drs James Fagin and Jeffrey Knauf as well as validating the other mutations (personal communication). Thyroid cells were maintained in RPMI 1640 medium (Cellgro, Manassas, VA, USA) supplemented with 5% fetal bovine serum (Hyclone, Logan, UT, USA), non-essential amino acids (Cellgro), sodium pyruvate (Cellgro), HEPES (Cellgro) and penicillin-streptomycin-amphotericin B (Cellgro) at 37 °C in a humidified atmosphere with 5% CO₂. We also purchased 293FT cells from Invitrogen and maintained them in DMEM as per the manufacturer's protocol along with 500 µg/ml neomycin (MP Biomedical, Solon, OH, USA).

Luciferase reporter gene analysis

Cells were plated in 12-well culture plates (Genesee Scientific, San Diego, CA, USA) at 1×10^5 cells/well. Once adhered, cells were transiently transfected using Lipofectamine 2000 (Invitrogen) with 25 ng pRL-CMV-renilla (Promega) and 1 µg pGL2/p21-luc 2280bp (provided by Dr Rebecca Chinery), or pGL3/RhoB-luc 1876bp (provided by Daniel Tovar, Institut Claudis Regaud, Toulouse, France) along with 0.5 µg each of MISSION shRNA pLKO.1 constructs HDAC1 through HDAC11 (Sigma–Aldrich). After 24 h, cells were lysed using Promega's Dual Luciferase assay kit per the manufacturer's protocol. Luciferase activity was measured using a Veritas luminometer (Promega) and the enzyme activity was normalized for transfection efficiency based upon renilla activity levels and reported as relative luminescent units \pm s.d. Comparisons were analyzed by two-tailed paired Student's *t*-test. $P < 0.05$ was considered statistically significant.

Lentivirus and infections

Self-inactivating shRNA lentiviruses were generated using MISSION shRNA pLKO.1 constructs that included a non-target control which was a random scrambled sequence (SHC002), *RhoB* 839 (clone NM_004040.2-839s1c1) and

was previously validated (Vishnu *et al.* 2012), *p21* 562 (clone NM_000389.2-562s1c1), *BIM* 537 and 541 (BCL2L11) (clones NM_138621.x-537s1c1, NM_138621.x-541s1c1), *HDAC1* (NM_004964.2-789s1c1), *HDAC6* 3384 and 3840 (NM_006044.2-3384s1c1, NM_006044.2-3840s1c1) (Sigma–Aldrich). Lentiviruses were packaged using 293FT cells via transfection of the pLKO.1 constructs along with packaging plasmids using OptiMEM and Lipofectamine 2000 (Invitrogen). The packaging plasmids were originally made by Didier Trono supplied by Addgene (Cambridge, MA, USA), which included pMDLg/pRRE (gag/pol) (plasmid #12251), pRSV-Rev (plasmid #12253), and pMD2.G (VSVG) (plasmid #12259). Supernatants were collected 72 h post-transfection, passed through a 0.45 µm PVDF syringe filter (Millipore, Bedford, MA, USA) and applied to cells for infection along with 5 µg/ml polybrene (American Bioanalytical, Natick, MA, USA). Cells were selected with puromycin (Fisher Scientific, Pittsburgh, PA, USA).

Proliferation assays

For dose out curves and lentiviral infected clones, cells were treated with belinostat, vorinostat, romidepsin or paclitaxel at the indicated doses and were counted on a Coulter Particle Counter (Beckman, Brea, CA, USA). When applicable, IC₅₀ was determined via extrapolation of 50% growth on log scale to the corresponding drug concentration. Using the ratio of the IC₅₀, the proportion of each compound needed in a combination dose was calculated. Experiments were then carried out using HDACi, paclitaxel and a fixed ratio combination of both at the indicated doses in clear-bottom black plates (Costar, Corning, NY, USA) and analyzed using the CyQUANT proliferation assay kit (Invitrogen) as per manufacturer's protocol for relative fluorescence units. Drug interactions were analyzed using CalcuSyn (Biosoft, Cambridge, UK). Determination of synergy, additivity or antagonism was based on the multiple drug effect equation of Chou and Talalay and was quantified by the combination index (CI). CI = 1 indicates an additive effect, <1 is synergy and >1 is antagonism (Chou & Talalay 1984).

Flow cytometry

Cells were grown to ~50% confluence prior to treatment. Floating cells were collected from the media and adhered cells were collected using Accutase (Innovative Cell Technologies, San Diego, CA, USA). For cell death analysis, cells were washed with cold PBS and resuspended in FACS binding buffer (PBS, 1% bovine serum albumin fraction V,

25 mM HEPES, 1 mM EDTA) followed by staining with propidium iodide (BD Pharmingen, San Jose, CA, USA). Annexin V was not used since the cells were strongly adherent. For cell cycle analysis, cells were resuspended in cold 0.5% glucose/PBS and fixed in 70% ethanol. For staining with propidium iodide, cells were resuspended in 0.1% triton X-100/PBS along with RNase A (Sigma-Aldrich). FACS analysis was performed on Accuri C6 flow cytometer (Accuri, Ann Arbor, MI, USA) using 100 000 events. Unstained cells were used as controls for setting the population parameters and overlay of histograms shows no deviation or drift of channels. More than a 5% change from the control was considered statistically significant. For cell cycle statistics, data was analyzed using MultiCycle AV (Phoenix Flow Systems, San Diego, CA, USA) with FCS Express plug-in (De Novo, Los Angeles, CA, USA).

RNA isolation and quantitative PCR

Total mRNA was isolated from cells using Purelink RNA isolation kit (Invitrogen) with DNase treatment per the manufacturer's protocol and the O.D. 260/280 ratio of the mRNA was at least 1.8. Two-step quantitative reverse transcriptase-mediated real-time PCR (qPCR) was used to measure changes in mRNA levels. The RT step was achieved by synthesizing cDNA using the High Capacity Reverse Transcription kit as per the manufacturer's protocol (Applied Biosystems). The PCR step was done using TaqMan Fast Universal PCR Master Mix (Applied Biosystems) and TaqMan FAM dye-labeled probes for *RhoB* (Hs00269660_s1), *p21* (Hs00355782_ml), *BIM* (BCL2L11, Hs00375807_ml), HDAC1 (Hs00606262_g1), HDAC2 (Hs00231032_m1), HDAC3 (Hs00187320_m1), HDAC4 (Hs01041648_m1), HDAC5 (Hs00608366_m1), HDAC6 (Hs00195869_m1), HDAC7 (Hs00248789_m1), HDAC8 (Hs00954353_g1), HDAC9 (Hs00206843_m1), HDAC10 (Hs00368899_m1), HDAC11 (Hs00978041_m1), and *POLR2A* (Hs00172187_ml). Data was normalized to *POLR2A* for each sample. Fold change values between nontargets and shRNA samples were calculated using the $\Delta\Delta C_t$ method (Schmittgen & Livak 2008).

Cell lysis and western blot analysis

Cells were grown to ~50% confluence prior to treatment. Floating and adhered cells were collected via scraping and lysed in M-PER extraction buffer (Pierce, Rockford, IL, USA) containing protease inhibitor cocktail (Roche) and phosphatase inhibitor (Pierce). Protein concentrations

were measured by bicinchoninic acid assay (Pierce) and 30 μ g were loaded on 4–12% Bis-Tris/MES gels (Invitrogen) and then transferred to 0.2 μ m Immobilon-P membranes (Millipore). The membranes were hybridized overnight at 4 °C with the following antibodies: BIM, PARP, Acetyl H3 L9 (Cell Signaling, Danvers, MA, USA); α -tubulin, acetyl α -tubulin, β -actin (Sigma-Aldrich); RhoB, p21, HDAC1, HDAC6 (Santa Cruz Biotechnologies). Secondary species-specific horseradish peroxidase-labeled antibodies were from Jackson Immunoresearch (West Grove, PA, USA). Detection was performed using Super-signal chemiluminescence kit (Pierce). Protein expression from Western blot analysis was quantitated using Image Quant 5.0 (Molecular Dynamics, GE Healthcare, Piscataway, NJ, USA). Blots were background corrected and normalized to loading controls.

Immunohistochemistry

A tissue microarray (TMA) was made from archival formalin fixed paraffin embedded samples under Mayo Clinic IRB approval. TMA tissues were cut into 5 mm sections, deparaffinized, hydrated, antigen retrieved and blocked with Diluent that contained Background Reducing Components (DAKO Cytomation, Glostrup, Denmark). Immunostaining was done with HDAC1 at 1:100 (Santa Cruz) and HDAC6 at 1:100 (Cell Signaling). The Envision Dual Labeled Polymer kit (DAKO Cytomation) was used according to the manufacturer's instructions and then lightly counterstained with Gill I hematoxylin (Sigma-Aldrich) before dehydration and mounting. Images were obtained at 20X using Scanscope XT (Aperio Technologies, Vista, CA, USA) and the staining of the TMA punches were scored using an algorithm in the Imagescope Software (Aperio Technologies) created by a histologist based upon signal intensity (0, 1+, 2+, 3+). *H* score was then calculated based upon signal intensity and percentage: $H = (1 + \% \times 1)(2 + \% \times 2)(3 + \% \times 3)$. Cases were excluded from the study if a section could not be assigned a score due to insufficient quantity of tumor tissue present.

Results

Downstream pathway differences of class I and II HDACi

Belinostat and vorinostat were hydroxamate class II/(I) (stronger class II than class I) HDACi while romidepsin was a cyclic peptide class I HDACi. Dose response curves for cell proliferation using four ATC cell lines were performed

with belinostat (PXD101), vorinostat (SAHA) or romidepsin (FK-228) ranging from 0.1 nM to 1 μ M for determination of IC₅₀ (50% inhibitory concentration). The class II/(I) inhibitors (Mai et al. 2005, Khan et al. 2008) belinostat yielded an IC₅₀ of 400 nM for both THJ-16T and THJ-21T and 250 nM for both THJ-29T and THJ-11T while vorinostat yielded an IC₅₀ of 250 nM for both THJ-16T and THJ-29T and 450 nM for THJ-11T and 500 nM for THJ-21T (Fig. 1A, panels 1 and 2). The class I inhibitor (Furumai et al. 2002), romidepsin yielded an IC₅₀ of 0.4 nM (Fig. 1A, panel 3) for each of the cell lines. Cell death effects of these HDACi were examined by flow cytometry and cell death was seen with belinostat and vorinostat treatments in all cell lines while romidepsin had no effect upon cell death in THJ-16T and THJ-29T. Belinostat induced cell death by 18–34% and vorinostat induced cell death by 10–19%. Romidepsin only induced cell death in THJ-11T and THJ-21T by ~10% (Fig. 1B). For both class II/(I) HDACi, THJ-29T exhibited greater sensitivity and the class I HDACi had no cell death effect. It should be noted that THJ-16T was *PI3KCA*, *TP53*, *Rb* mutant, THJ-11T was *KRAS* mutant, THJ-21T was *BRAF*, *TP53*, *Rb* mutant and THJ-29T was *Rb* mutant which may have influenced responses to each of the HDACi (Marlow et al. 2010). Apoptosis was examined via PARP cleavage. Belinostat and vorinostat treatments induced cleaved PARP in all four ATC cell lines while romidepsin treatment

did not in THJ-16T and THJ-29T (Fig. 1C). Previous publications demonstrated that vorinostat induced apoptosis via upregulation of the proapoptotic Bcl2-interacting mediator of cell death, BIM, which triggered cytochrome c release from the mitochondria leading to apoptosis (Zhao et al. 2005). We found that the BIM isoform, BIM_{EL} (extended length) (Ramesh et al. 2009) was strongly induced by Class II/(I) HDACi, belinostat, and vorinostat in all four cell lines, and weakly with Class I HDACi romidepsin in THJ-11T and THJ-21T (Fig. 1C) with no change in XIAP, survivin, Bax, p-Bcl2 (data not shown). Based upon previous studies of romidepsin's effects in ATC cells and that RhoB and p21 are repressed by HDAC1, they were also examined by western blot (Sambucetti et al. 1999, Wang et al. 2003, Marlow et al. 2009, 2010). All three HDACi induced RhoB protein expression while p21 expression was dependent upon the HDACi and cell line. Romidepsin induced p21 in all four cell lines while belinostat induced p21 in THJ-21T and vorinostat induced p21 in THJ-11T and THJ-21T. Since BIM degradation can be regulated by Erk signaling (Akiyama et al. 2009, Chakraborty et al. 2013), p-Erk and p-Akt (data not shown) expression was examined and no consistent change in expression was found within or across the four ATC cell lines examined (Fig. 1C). To test if THJ-16T and THJ-29T functioned differently at the transcriptional level, *RhoB* and *p21* reporter activity were examined.

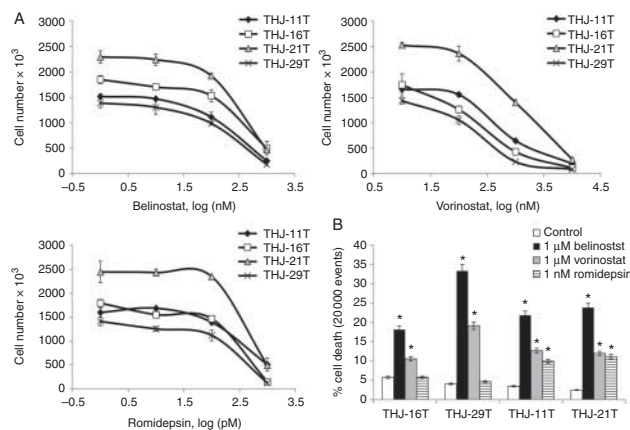


Figure 1

Comparison of class I and II HDAC inhibitors in ATC cell lines. For dose response curves, ATC cells were plated in triplicate in 12-well culture plates at 2×10^4 cells/well and treated for 72 h. Data was plotted on log scale for drug concentrations vs cell number \pm s.d. (A) The class II/(I) hydroxamate inhibitors: belinostat (PXD101) yielded IC₅₀ of 400 nM for both THJ-16T and THJ-21T and 250 nM for both THJ-11T and THJ-29T (panel 1). Vorinostat (SAHA) yielded IC₅₀ of 250 nM for both THJ-16T and THJ-29T and 450–500 nM for THJ-11T and THJ-21T (panel 2). The cyclic peptide class I inhibitor: romidepsin (FK-228) yielded IC₅₀ of 0.4 nM for all four cell lines

(panel 3). (B) For cell death, cells were grown to ~50% confluence and treated with either 1 μ M belinostat (Bel), 1 μ M vorinostat (Vor) or 1 nM romidepsin (Rom) for 72 h prior to flow cytometry with propidium iodide. Data is plotted as average percent cell death within 20 000 events \pm s.d. **P* < 0.05 was considered statistically significant when compared to DMSO control. (C) For western blots, cells were treated for 24 h and analyzed by western blot for p-Erk, RhoB and p21. BIM_{EL} and cleaved PARP were indicators of apoptosis and β -actin was used as a loading control.

All three HDACi induced *RhoB* (approximately seven- to 27-fold) and *p21* (approximately four- to ninefold) transcription (Supplementary Figure 1). Endogenous *RhoB* (approximately four- to sevenfold, panel 1) and *p21* (approximately seven- to 18-fold, panel 2) mRNA levels were also induced by all three HDACi in all four cell lines (Fig. 2A, panels 1 and 2). *BCL2L11* (*BIM*) mRNA was also measured with an induction of approximately two- to sixfold with greater effects seen with belinostat and

vorinostat in all four cell lines (Fig. 2A, panel 3). Thus, in order to address the inconsistencies in mRNA levels and protein expression, protein stability was assessed using a time course with or without the proteasome inhibitor, MG132 using THJ-16T and THJ-11T as a representative. As expected, RhoB expression was consistently upregulated by 6 h in both cell lines for all three HDACi (B, C and D). Interestingly, p21 protein in THJ-16T was greatly induced by belinostat at 12 h and completely degraded by 24 h,

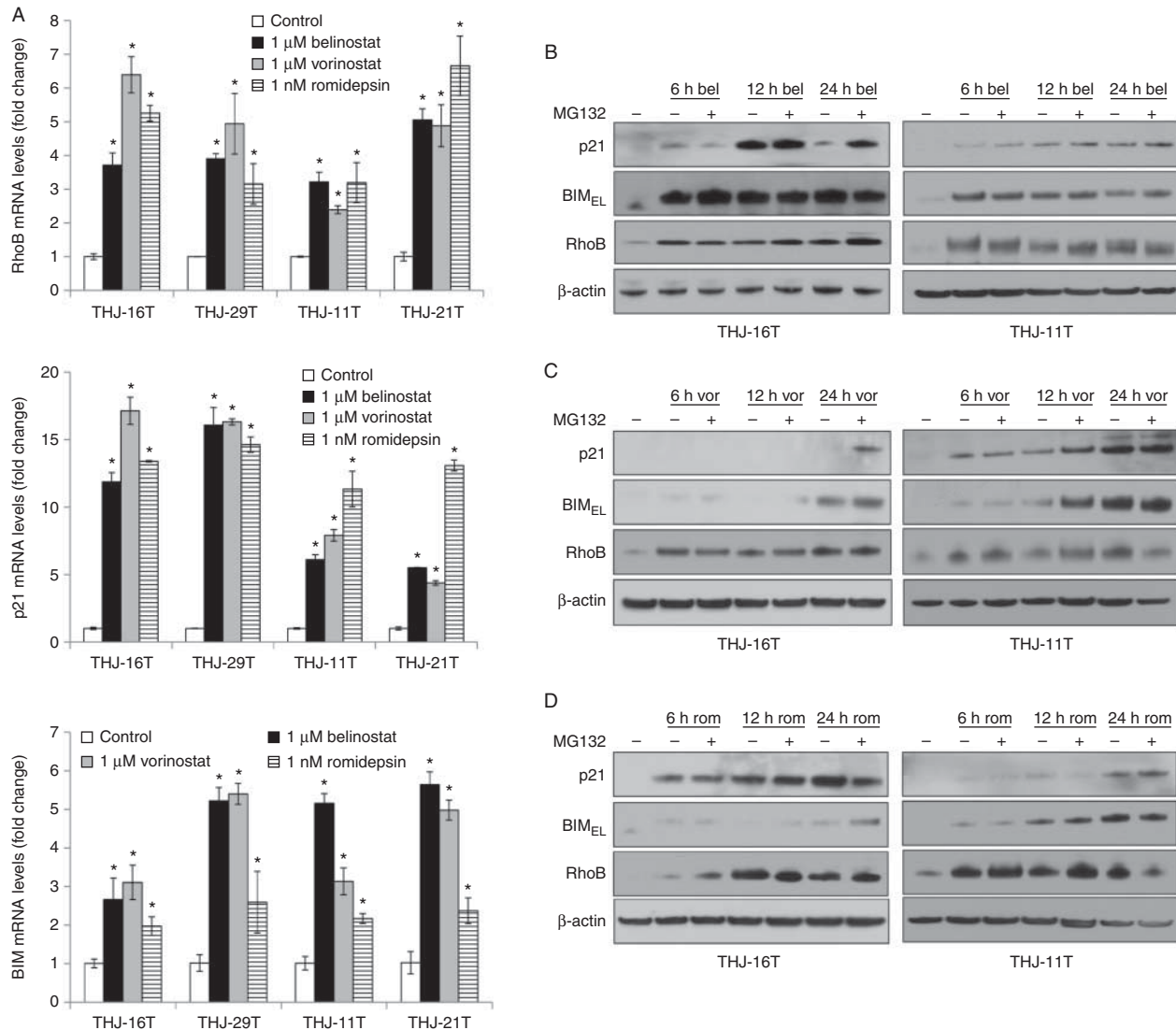


Figure 2

HDAC inhibitors have different p21/BIM_{EL} mRNA and protein expression. (A) For verification of transcriptional activation of *RhoB* and *p21* (Supplementary Figure 1, see section on supplementary data given at the end of this article), qPCR was done in cells treated for 24 h with HDACi (panels 1 and 2). qPCR was also performed for *BCL2L11* (*BIM*) mRNA levels and elevated in all HDACi treated cells (panel 3). Data was plotted as fold change \pm s.d. * $P < 0.05$ was considered statistically significant when

compared to DMSO control. (B) Western blot analysis of THJ-16T and THJ-11T cells treated with belinostat alone or in combination with 1 nM MG132 (a proteasome inhibitor) at the indicated time points was done for monitoring protein stability. (C) Western blot analysis was performed for vorinostat alone or in combination with 1 nM MG132. (D) Western blot analysis was performed for romidepsin alone or in combination with 1 nM MG132.

which could be rescued by the proteasome inhibitor, MG132. In THJ-11T, p21 protein levels remained consistent over the time course. BIM_{EL} protein levels were upregulated by belinostat as early as 6 h and BIM_{EL} protein was not targeted for proteasome degradation (Fig. 2B). Vorinostat had not induced p21 protein in THJ-16T at any time point indicating rapid degradation except when MG132 rescued p21 at 24 h while p21 remained upregulated as early as 6 h in THJ-11T. By 24 h in THJ16T, vorinostat upregulated BIM_{EL} protein levels and it was not targeted for proteasome degradation. However, in THJ-11T, BIM_{EL} protein levels were increased by 6 h and at 12 h it was further enhanced with MG132, which indicated some proteasome degradation, but this did not occur at 24 h (Fig. 2C). With romidepsin in THJ-16T, p21 protein was induced by 6 h and remained elevated regardless of proteasome inhibition by MG132 while BIM_{EL} protein was not seen until 24 h with MG132, which indicated rapid degradation. Interestingly, p21 was not elevated until 24 h in THJ-11T while BIM_{EL} protein levels were seen as early as 6 h with no effects seen with MG132 (Fig. 2D). Thus, if degraded, both p21 and BIM_{EL} protein can be rescued by MG132. In order to demonstrate that the HDACi were RhoB-dependent, *RhoB* was silenced using *RhoB839* shRNA; specificity of this shRNA against RhoB has been previously demonstrated (Marlow et al. 2009, 2010, Vishnu et al. 2012). The level of *RhoB* silencing in these models ranged from 35 to 65% as examined by qPCR (Supplementary Figure 2, see section on supplementary data given at the end of this article). When *RhoB* was silenced during HDACi treatment, proliferative inhibition was reversed by ~40–100%

(Fig. 3A). Using THJ-16T and THJ-21T as representative, western blots confirmed that RhoB was silenced by *RhoB* shRNA and that p21 induced by romidepsin was blocked when upstream *RhoB* was silenced. Induced BIM_{EL} was also blocked with *RhoB* silencing (Fig. 3B). Therefore, upregulation of *RhoB* was necessary for p21 and BIM_{EL} expression.

Combinatorial therapy with HDACi and paclitaxel

An assortment of findings which included, RhoB-dependent antitumor synergy with paclitaxel and a PPAR γ agonist (Marlow et al. 2009), paclitaxel stabilizing BIM_{EL} expression in breast cancer models (Akiyama et al. 2009), and having some efficacy in patients with ATC (Ain et al. 2000) inspired us to combine paclitaxel with the three HDACi used in this study. We tested each HDACi in combination with paclitaxel for antitumor synergy with the expectation of observing RhoB-dependent antitumor synergy. The concentration at which 50% inhibition of cell proliferation (IC₅₀) for paclitaxel was determined and yielded an IC₅₀ of 0.5 nM for THJ-16T, 2 nM for THJ-29T and 4 nM for THJ-11T and THJ-21T (Supplementary Figure 3, see section on supplementary data given at the end of this article). Synergy between each HDACi and paclitaxel was assessed using the median effects model of Chou & Talalay (1984). Belinostat combined with paclitaxel yielded synergy in THJ-16T (CI_{ED50}=0.12), THJ-29T (CI_{ED50}=0.47), THJ-11T (CI_{ED50}=0.89) and THJ-21T (CI_{ED50}=0.47) as shown by the left shifts of the dose curves (Fig. 4A). Vorinostat combined with paclitaxel also yielded synergy with CI_{ED50}=0.49, CI_{ED50}=0.36,

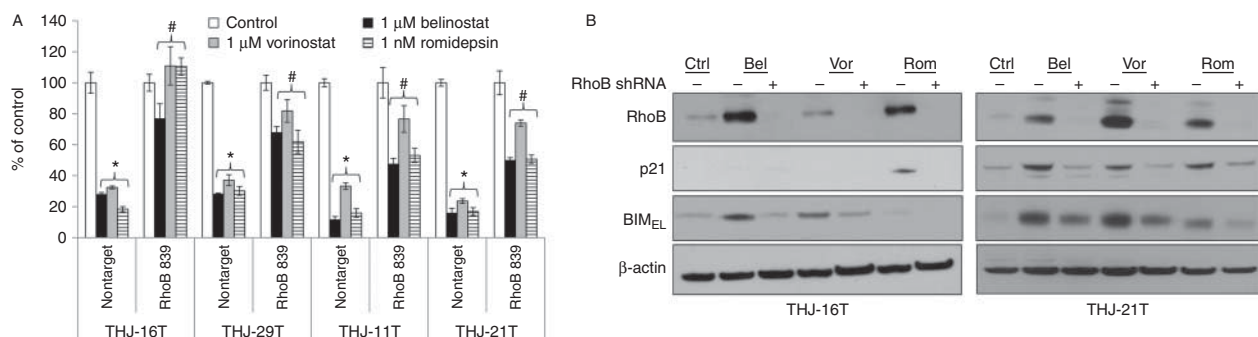


Figure 3

Both p21 and BIM are RhoB dependent. (A) Nontarget and RhoB 839 shRNA silenced cells were plated in triplicate in 12-well culture plates at 2×10^4 cells/well and treated for 72 h with 1 μ M belinostat, 1 μ M vorinostat and 1 nM romidepsin. Data was plotted as cell number \pm s.d. * $P < 0.05$ was considered statistically significant when compared to untreated control.

$P < 0.05$ was considered statistically significant when compared to applicable nontarget treatment. (B) Western blot analysis of nontarget and RhoB 839 shRNA cells treated for 24 h showed that BIM_{EL} and p21 were blocked when RhoB was silenced. β -actin was used as a loading control.

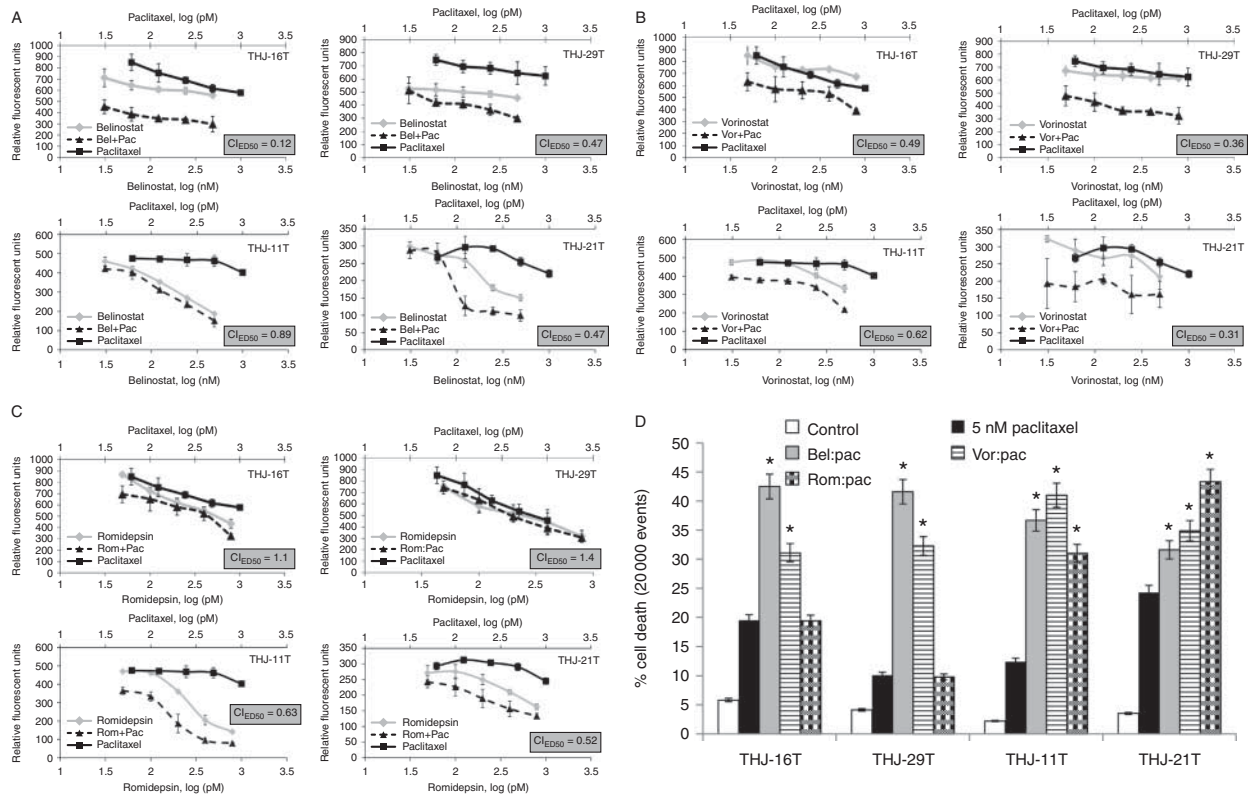


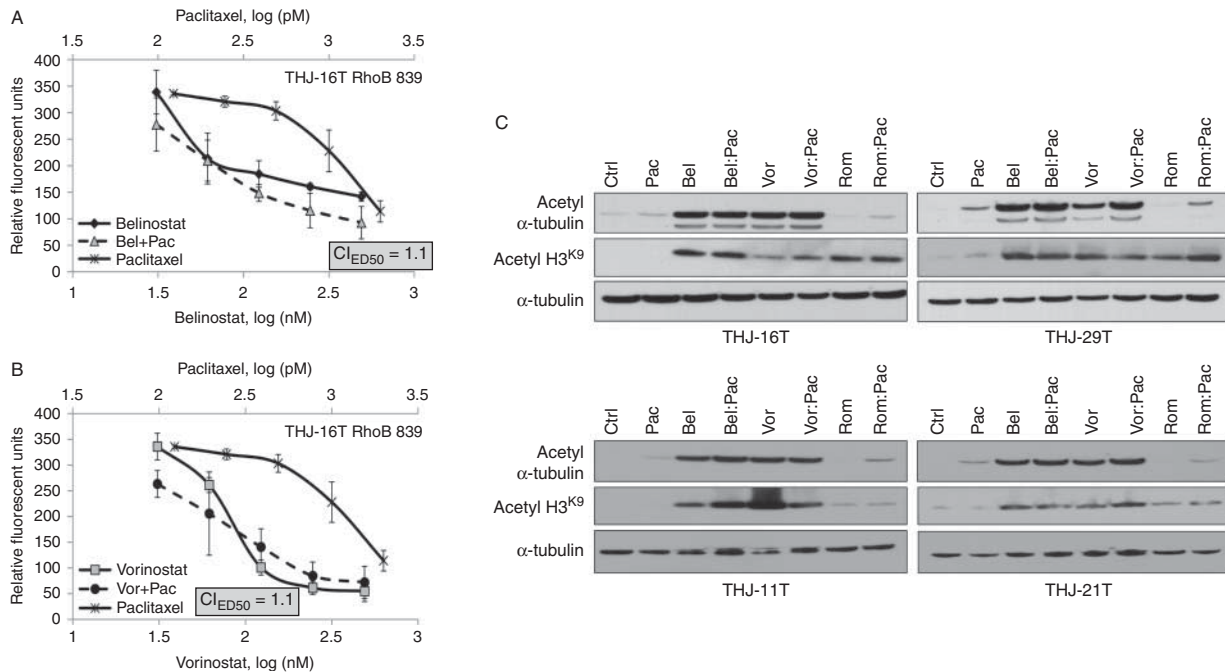
Figure 4

Synergy of HDAC inhibitors and paclitaxel were dependent upon presence of BIM expression. ATC cells were plated at 2500 cells/well and treated for 72 h prior to CyQUANT analysis. Experiments were carried out using HDAC inhibitors, paclitaxel and a fixed ratio combination of both at a variety of different doses as indicated. (A) Belinostat in combination with paclitaxel demonstrated synergy as indicated by the left shift and CI_{ED50} value < 1.0 . ED_{50} is effective dose at 50% (B) Vorinostat also had synergy when combined with paclitaxel as indicated by CI_{ED50} value < 1.0 . (C) Romidepsin did not have synergy (CI_{ED50} value > 1.0) when combined with paclitaxel in THJ-16T and THJ-29T, which did not have BIM_{EL} expression (panels 1 and 2).

$CI_{ED50} = 0.62$ and $CI_{ED50} = 0.31$ respectively (Fig. 4B). However, combinatorial romidepsin and paclitaxel demonstrated no synergy and no left shift ($CI_{ED50} = 1.1$, $CI_{ED50} = 1.4$) in THJ-16T and THJ-29T while synergy was observed in THJ-11T ($CI_{ED50} = 0.63$) and THJ-21T ($CI_{ED50} = 0.52$) (Fig. 4C). CI values of < 1 are considered synergistic. Cell death analysis with combinatorial therapy demonstrated similar results with enhanced cell death with the Class II/I HDACi combined with paclitaxel in all four cell lines ($\Delta 15$ – 40%), but not with romidepsin in THJ-16T and THJ-29T where BIM_{EL} was not elevated. Enhanced cell death with romidepsin and paclitaxel was seen in THJ-11T ($\Delta 18\%$) and THJ-21T ($\Delta 18\%$) (Fig. 4D). Thus, in HDACi treated cells where BIM_{EL} was elevated, apoptosis and combinatorial therapy antitumor synergy occurred regardless of p21 expression levels. The combinatorial effect with

On the other hand, romidepsin did have synergy with paclitaxel in THJ-11T and THJ-21T, which do have BIM_{EL} expression (panels 3 and 4) and have KRAS and BRAF mutations respectively. (D) Cell death analysis after 72 h with combinatorial therapy demonstrated enhanced cell death with the Class II HDACi, but not with romidepsin when compared to paclitaxel alone in THJ-16T and THJ-29T. Cell death was observed with all HDACi for both THJ-11T and THJ-21T. Data is plotted as average percent cell death within 20 000 events \pm s.d. * $P < 0.05$ was considered statistically significant when compared to DMSO control.

belinostat could be reversed when *RhoB* was silenced in representative THJ-16T cells ($CI_{ED50} = 1.1$) with the loss of a leftward curve shift (Fig. 5A). As well, the combinatorial effect with vorinostat could be reversed when *RhoB* was silenced in THJ-16T ($CI_{ED50} = 1.1$) also (Fig. 5B). A previous publication using valproic acid (class I/II HDACi) in ATC cells indicated that paclitaxel via microtubule stabilization promoted acetylated α -tubulin as the mechanism of synergy (Catalano *et al.* 2007). We thus examined belinostat or vorinostat in combination with paclitaxel for this potential explanation of synergy. However, there was no consistent enhancement of acetyl α -tubulin in the presence of paclitaxel in either of the four cell lines (Fig. 5C). Thus, our results indicated that loss of combinatorial synergy was dependent upon *RhoB* signaling and not acetyl α -tubulin.

**Figure 5**

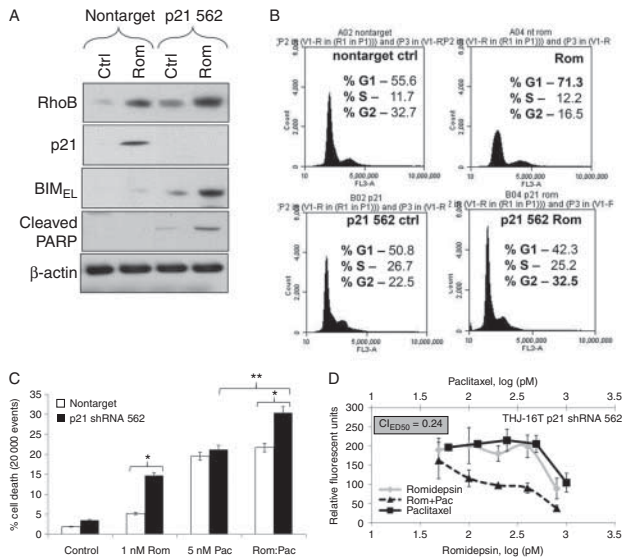
Combinatorial synergy is dependent upon RhoB and not acetylated α -tubulin. (A) Using THJ-16T, belinostat in combination with paclitaxel lost its synergy when RhoB was silenced as indicated by CI_{ED50} value > 1.0 . (B) Vorinostat in combination with paclitaxel also lost its synergy when RhoB was silenced as indicated by CI_{ED50} value > 1.0 . (C) ATC cells were

treated with HDACi and paclitaxel alone or in combination for 24 h to verify HDAC inhibitor and paclitaxel activities via increased expression of acetyl α -tubulin when treated alone or in combination. α -tubulin was used as a loading control.

Flipping the RhoB \rightarrow p21 and RhoB \rightarrow BIM_{EL} pathway switch

To identify the role of p21 upregulation in romidepsin treated cells, p21 was silenced. p21 shRNA constructs were screened by qPCR and *p21* clone 562 was identified to effectively silence *p21* mRNA ($\sim 65\%$) (Supplementary Figure 2). Western blot analysis using the *p21* 562 construct in THJ-16T cells showed that romidepsin treatment induced RhoB, but when *p21* was silenced, BIM_{EL} and PARP cleavage were induced (Fig. 6A). Cell cycle analysis showed that romidepsin treatment shifted nontarget control cells to G1 phase ($\sim \Delta 15.7\%$). However, when *p21* was silenced with romidepsin, G2 phase was increased by $\sim \Delta 10\%$ with a sub-G0 population to the left of the histogram (Fig. 6B). Cell death analysis by flow cytometry in THJ-16T showed that when *p21* was silenced, cell death was evoked in romidepsin treated cells by $\Delta 12\%$ and that combinatorial cell death effects enhanced by $\sim 10\%$ with an overall cell death of 30% (Fig. 6C). Combinatorial effects were then examined via cell proliferation and romidepsin with paclitaxel showing synergy ($CI_{ED50} = 0.24$) when *p21* was silenced (Fig. 6D). Thus, silenced p21 allowed BIM_{EL} to

be expressed at the protein level reversing the phenotype to re-establish synergy. We next tested whether silencing BIM_{EL} would lead to loss of synergy. BIM_{EL} shRNA constructs were screened by qPCR and BIM_{EL} clones 537 and 541 were identified to effectively silence BIM mRNA by $\sim 40\%$ and $\sim 50\%$ respectively (Supplementary Figure 2). Western blot analysis of THJ-16T using BIM_{EL} 541 construct showed belinostat/vorinostat treatments still induced RhoB, but when BIM_{EL} was silenced, PARP cleavage was lost. In the presence of BIM shRNA, BIM_{EL} was silenced and p21 protein expression was induced in the presence of both belinostat and vorinostat treatments (Fig. 7A). Cell cycle analysis showed that belinostat and vorinostat increased the percent of cells in G2 phase by $\sim \Delta 19\%$ and induced a sub-G0 subpopulation vs that of nontarget control cells. However, when BIM_{EL} was silenced in treated cells, the G1 phase was shifted by $\sim \Delta 17.7$ and $\Delta 15.7\%$ with diminished sub-G0 populations respectively (Fig. 7B). Furthermore, in belinostat and paclitaxel treated THJ-16T cells with BIM_{EL} silenced, synergy was lost ($CI_{ED50} = 1.1$) (Fig. 7C). Thus, combinatorial synergy can be reversed by silenced BIM_{EL} presumably via re-expression of p21 protein leading to cytostasis.

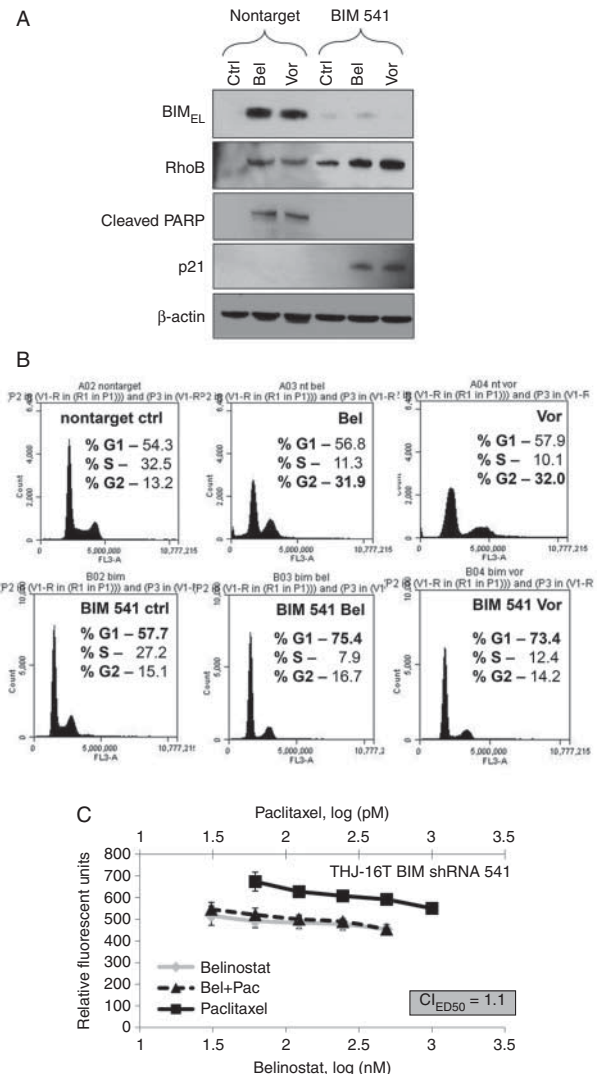
**Figure 6**

Silencing p21 in the presence of romidepsin shifts RhoB to the BIM pathway. (A) Western blot analysis of the p21 562 construct in THJ-16T cells demonstrated that RhoB remained induced upon romidepsin treatment while BIM_{EL} and PARP cleavage was induced when p21 was silenced. β-actin was used as a loading control. (B) Cell cycle analysis after 72 h with romidepsin treatment was done to examine shifting in the G1 phase and G2 phase reversal. (C) Cell death analysis with 72 h treatment showed that romidepsin does not induce cell death unless p21 is silenced. * $P < 0.05$ was considered statistically significant when compared to applicable nontarget ** $P < 0.05$ was considered statistically significant when compared to paclitaxel alone. (D) When p21 was silenced, romidepsin and paclitaxel showed combinatorial synergy in both cell death and cell growth inhibition as indicated by Cl_{ED50} value < 1.0 .

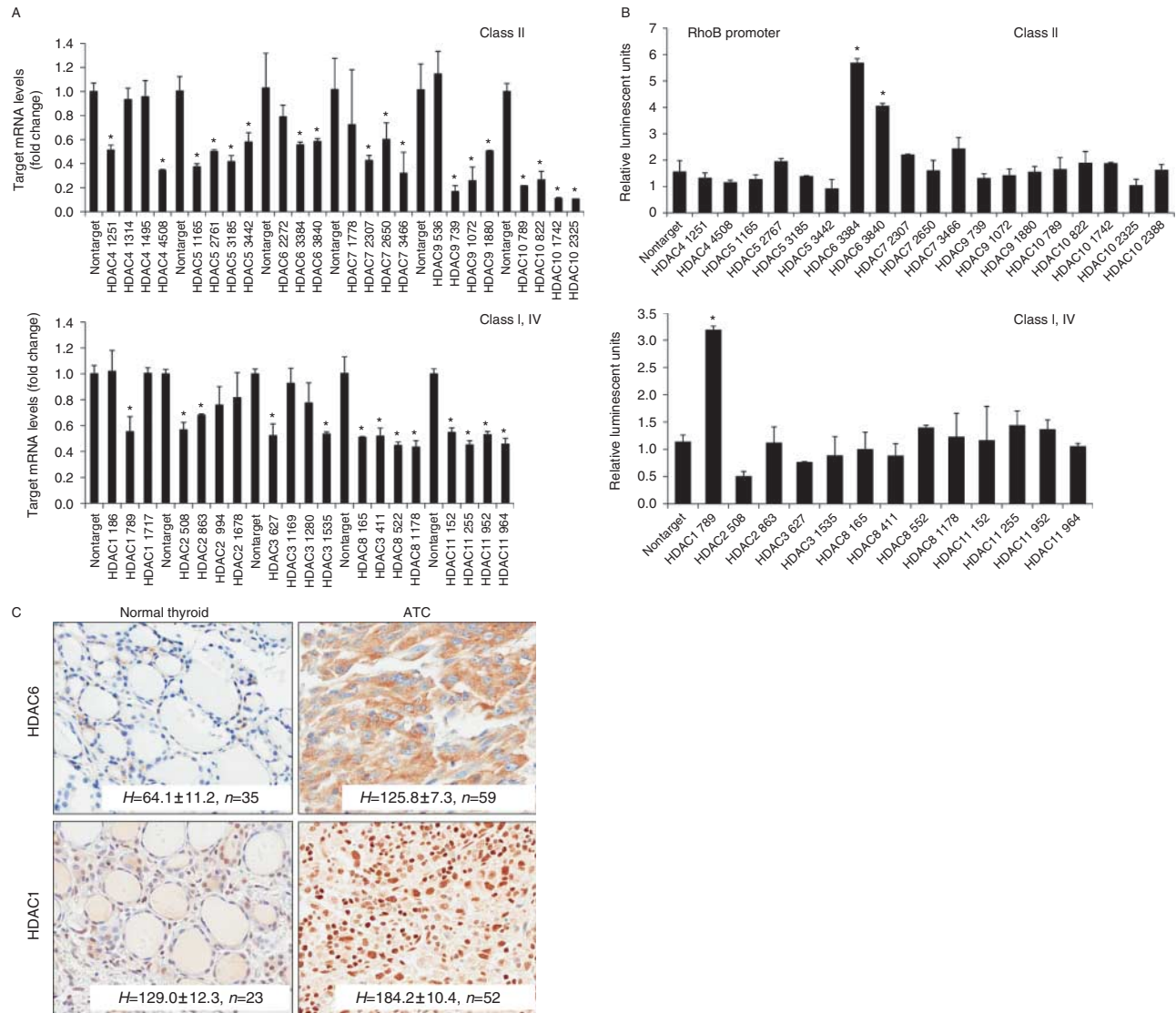
HDAC1 and HDAC6 are repressors of RhoB

Since there were differential HDACi effects on RhoB signaling leading to p21 or BIM_{EL}, all HDACs were examined from classes I, II and IV. Using multiple shRNA constructs against HDAC1 to 11, THJ-16T cells were transiently transfected and the level of silencing was examined by qPCR for the corresponding HDAC (Fig. 8A). Luciferase reporter assay of the RhoB promoter co-transfected with each of the verified HDAC shRNAs were used to screen transcriptional regulation for HDAC 1–11. Activation of the RhoB promoter was observed when HDAC1 was silenced by clone 789 and HDAC6 clones 3384 and 3840 (Fig. 8B). For verification, THJ-29T was tested using positive and negative constructs from the panel. Again, HDAC1789, HDAC6 3384 and 3840 showed RhoB promoter activity while the non-effective HDAC shRNAs did not (Supplementary Figure 4, see section on supplementary data given at the end of this article). Thus, both HDAC1 and HDAC6 repressed the RhoB promoter and to our knowledge, this is the first report of RhoB repression by

HDAC6. For clinical relevance, IHC was performed on patient normal and ATC tissues. Both HDAC6 ($H = 125.8$, $n = 59$) and HDAC1 ($H = 184.2$, $n = 52$) were overexpressed in ATC as compared to normal tissues ($H = 64.1$ ($n = 35$), $H = 129.0$ ($n = 23$) respectively), which indicated that HDAC6 and HDAC1 may be viable molecular therapeutic targets (Fig. 8C). Direct targeting of HDAC1 or HDAC6 via shRNA was used to mimic the HDACi to further verify transcriptional suppression of RhoB, BIM_{EL} and p21.

**Figure 7**

Silencing BIM in the presence of belinostat and vorinostat shifts RhoB to the p21 pathway. (A) Western blot analysis using the BIM 541 construct in THJ-16T cells was examined for effects upon downstream targets. PARP cleavage was lost when BIM was silenced and p21 expression was induced. β-actin was used as a loading control. (B) Cell cycle analysis after 24 h treatment with belinostat and vorinostat treatment was done to examine shifting in the G2 phase and G1 phase reversal. (C) Combinatorial synergy was lost with belinostat and paclitaxel when BIM_{EL} was silenced.

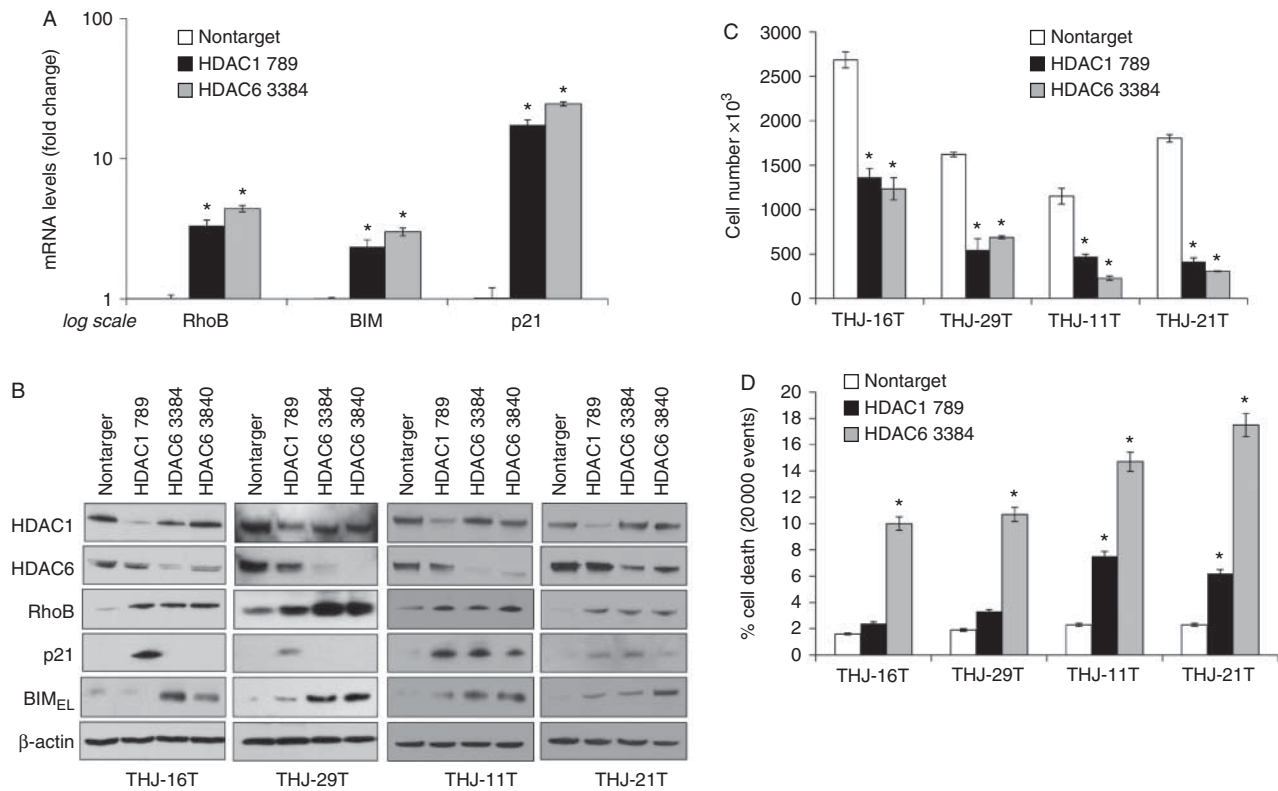
**Figure 8**

Identification of HDAC1 and HDAC6 as repressors of RhoB. (A) THJ-16T cells were transiently transfected with MISSION shRNA pLKO.1 constructs: nontarget, HDAC1 (clones NM_004964.2), HDAC2 (clones NM_001527.1), HDAC3 (clones NM_003883.2), HDAC4 (clones NM_006037.2), HDAC5 (clones NM_005474.3), HDAC6 (clones NM_006044.2), HDAC7 (clones NM_015401.1), HDAC8 (clones NM_018486.1), HDAC9 (clones NM_014707.1), HDAC10 (clones NM_032019.4), and HDAC11 (clones NM_024827.1). The construct clone numbers are as indicated. qPCR was performed for each set of HDACs in order to examine level of silencing. (B) Luciferase RhoB reporter assay for screening transcription regulation

by HDACs from class I, II and IV. THJ-16T cells were transiently transfected with renilla, RhoB-luc and verified MISSION shRNA pLKO.1 constructs as indicated. Luciferase data was normalized for transfection efficiency based upon renilla activity levels and reported as relative luminescent units \pm s.d. Comparisons were analyzed by two-tailed paired Student's *t*-test. $*P < 0.05$ was considered statistically significant as compared to nontarget control. (C) IHC of patient normal and ATC tissue for HDAC1 and HDAC6 showed strong staining for both HDACs in tumor tissue as indicated by *H* score \pm s.d. Sample size (*n*) was as indicated.

Using the *HDAC1 789* and *HDAC6 3384* clones in THJ-16T, qPCR revealed that *RhoB*, *p21* and *BIM* mRNA were all induced when *HDAC1* or *HDAC6* were silenced (Fig. 9A). For protein expression, silenced *HDAC1* or *HDAC6* led to RhoB induction in all four cell lines. Unique to THJ-16T and THJ-29T cells, silenced *HDAC1* led to p21

induction only while silenced *HDAC6* led to *BIM_{EL}* induction only. On the other hand, silenced *HDAC1* or *HDAC6* induced both p21 and *BIM_{EL}* in *KRAS* mutant THJ-11T and *BRAF* mutant THJ-21T cells (Fig. 9B). These four cell lines were also growth inhibited by ~45–65% by *HDAC1* or *HDAC6* shRNAs (Fig. 9C). Flow cytometry of the

**Figure 9**

Downstream effects of HDAC1 and HDAC6. (A) qPCR of RhoB, p21 and BIM in HDAC1 and HDAC6 silenced THJ-16T cells show that all three mRNAs are upregulated. (B) Western blot analysis of nontarget, HDAC1 789, HDAC6 3384 and HDAC6 3840 shRNA clones were examined for differential downstream targets effects. β -actin was used as a loading control. (C) Nontarget and HDAC shRNA cells were selected for 24 h and then plated

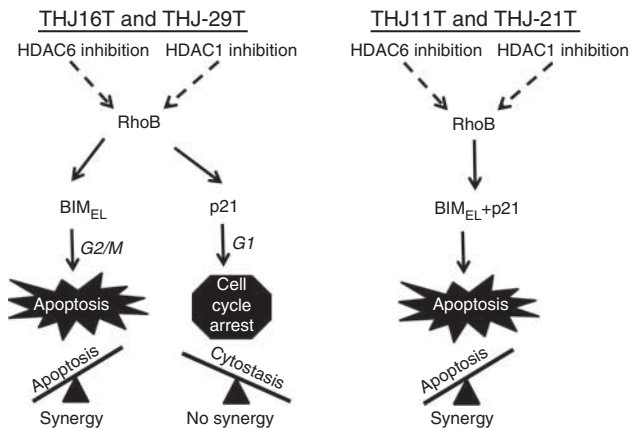
in triplicate in 12-well culture plates at 2×10^4 cells/well for 72 h. Data was plotted as cell number \pm s.d. * $P < 0.05$ was considered statistically significant when compared to nontarget control. (D) After 36 h selection, cells were plated for cell death analysis and incubated for 72 h prior to flow cytometry with propidium iodide.

shRNA clones showed that cell death was induced by ~ 10 –18% with *HDAC6* silenced in the four cell lines. However, no cell death was detected upon silenced *HDAC1* in THJ-16T and THJ-29T, which had p21 but no BIM_{EL} expression. Conversely, cell death was detected upon silenced *HDAC1* in THJ-11T (7%) and THJ-21T (6%) where both p21 and BIM_{EL} expression were elevated (Fig. 9D). Overall, the HDAC shRNA data corroborated the effects seen with belinostat, vorinostat, and romidepsin.

Discussion

In this study, cell proliferation was inhibited using both class I and class II(I) HDAC inhibitors in a dose responsive fashion in four recently developed patient derived ATC cell lines harboring different driver mutations (*BRAF*, *PI3KCA*, *KRAS*, *APC*). Clear distinctions between cell lines in response to the different HDACi arose related to cell cycle regulation (G0/G1 vs G2/M) dictating cytostasis or cell

death, mediators of cell cycle regulation (p21 vs BIM_{EL}), and response to combinatorial therapeutic (synergy vs no synergy). These findings were dependent on whether upregulated RhoB was followed by either p21 exclusively or BIM_{EL} with/without p21. This differential protein expression was regulated in part by the proteasome since both *BIM* and *CDKN1* mRNA were upregulated by both class I and II/I HDACi. In generalizing the results, G2/M arrest, apoptotic cell death and paclitaxel combinatorial synergy resulted with upregulated BIM_{EL} protein regardless of p21 protein status. This occurred in response to class II/I HDACi in all cell lines and class I HDACi in THJ11T and THJ-21T but not THJ-16T and THJ29T. Conversely, when romidepsin, the class I HDACi, induced only p21 protein (THJ-16T and THJ-29T), G0/G1 cell cycle arrest with cytostasis occurred and p21 was responsible for lack of synergy with combined paclitaxel therapy. These findings were summarized in our models as shown in Fig. 10. In the past, we and others have observed RhoB-mediated

**Figure 10**

Divergent RhoB pathways. RhoB expression was regulated by both HDAC1 and HDAC6 and inhibition of these HDACs in ATC led to the dominant pathway downstream of RhoB. If BIM_{EL} was induced by RhoB, then it led to apoptosis/cell death and combinatorial synergy. If p21 was exclusively induced by RhoB, then it led to cytostasis and no combinatorial synergy. These pathways acted as a seesaw and the dominant pathway determined the fate of the cell.

induction of p21 (Du & Prendergast 1999, Marlow *et al.* 2009) or BIM_{EL} (Srougi & Burrige 2011). Alternatively, HDACs directly suppressed p21 and BIM_{EL} transcription by binding to their respective promoters (Wang *et al.* 2004, Mazieres *et al.* 2005, Zhao *et al.* 2005, Chan *et al.* 2013). Belinostat and vorinostat have been shown to induce p21 transcription and translation that was p53-dependent in thyroid cancer cells via the zinc transcription factor, Sp1 (Wang *et al.* 2004, Mitsiades *et al.* 2005, Chan *et al.* 2013). In our models, p21 expression was induced by these agents in both p53 WT (THJ-11T, THJ-29T) and p53 mutant (THJ-16T, THJ-21T) cells. Furthermore, vorinostat had been shown in other cancer models to recruit E2F1 to the *BIM* promoter for inducing BIM_{EL} expression (Zhao *et al.* 2005). Our current study demonstrated both HDACi and RhoB-dependent transcriptional induction of p21 and BIM_{EL} mRNA, whereby RhoB transcription was also HDACi-dependent (HDACi RhoB p21 and/or BIM_{EL}). Moreover, transcription of the *RhoB* promoter can be activated by farnesyltransferase and geranylgeranyl transferase inhibitors via HDAC1 dissociation (Delarue *et al.* 2007). HDAC1 repressed *RhoB* by binding to an inverted CCAAT box in the *RhoB* promoter and its regulation was independent of Sp1 (unlike p21) (Wang *et al.* 2003, 2004, Delarue *et al.* 2007). In our study, we also saw HDAC1 repression of *RhoB* and to our knowledge, this was the first report of *RhoB* repression by HDAC6. However, it had been reported that with trapoxin A (pan-HDACi) treatment in

lung and breast tumor cell lines, HDAC6 had no association on the *RhoB* promoter (Wang *et al.* 2004). For clinical relevance, we demonstrated that HDAC6 and HDAC1 were elevated in ATC vs normal thyroid tissue. Unlike HDAC1, which resided in the nucleus, HDAC6 remained predominantly in the cytoplasm associated with microtubules and the cytoskeleton (Boyault *et al.* 2007, Li, *et al.* 2008, Kaliszczak *et al.* 2013). The mechanism by which HDAC6 inhibition led to upregulation of RhoB transcription has yet to be identified. It had been reported that transcriptional regulation of RhoB in response to UV irradiation and farnesyltransferase inhibitors was associated with the recruitment of the transcriptional nuclear factors NF-Y and c-Jun, and histone acetyltransferase p300 to the CCAAT or inverted CCAAT box in the proximal *RhoB* promoter (Ahn *et al.* 2011, Kim *et al.* 2014). We hypothesized that a direct cross-talk between HDAC6 and p300 (opposing enzymatic activities) could be a mechanism to regulate RhoB gene transcription upon HDAC6 inhibition. HDAC6 predominantly deacetylates non-histone proteins, including α -tubulin; p300 acetylation of HDAC6 results in decrease of HDAC6 deacetylase activity thereby tubulin deacetylation and suppression of Sp1 transcriptional activity. Thus, p300 may regulate the activity of Sp1 indirectly through HDAC6 in addition to its direct modification of Sp1 (Ahn *et al.* 2011). With HDAC6 suppression, this RhoB transcriptional complex may become re-engaged. In summary, we had uncovered novel regulation of RhoB by HDAC6 and HDAC1 which then modulated another novel switch co-regulating p21 and BIM_{EL}. Interestingly, HDAC6 is the only member, within the histone deacetylase family, that harbored a full duplication of its deacetylase homology region followed by a specific ubiquitin-binding domain at the C-terminus (Boyault *et al.* 2007, Li *et al.* 2013). High-affinity binding of HDAC6 to ubiquitin was shown to hinder the recognition of ubiquitinated proteins by other ubiquitin-binding factors and to delay their processing by the ubiquitin proteasomal subunit (Boyault *et al.* 2006). Therefore, HDAC6 blocked proteasome degradation. Others have reported that p21 and BIM_{EL} were degraded via proteasomal degradation (Akiyama *et al.* 2009, Altmann, *et al.* 2012), which may explain the absence of p21 protein in the class II(I) HDACi treated cells. In addition, *BIM* transcription was regulated by FoxO3a and RUNX3 and its degradation was regulated by Erk signaling (Akiyama *et al.* 2009, Chakraborty *et al.* 2013) and that alterations in their activities may be HDACi-specific. BIM_{EL} contained two ubiquitination sites and three ERK phosphorylation sites and belinostat had been shown to inhibit p-Akt and p-Erk signaling

(Chan *et al.* 2013). Phosphorylation by p-Erk targeted BIM_{EL} for ubiquitination and proteosomal degradation (Akiyama *et al.* 2009). Hence, decreased p-ERK will stabilize BIM_{EL} expression when HDAC6 was dissociated. One study had shown that the use of Mek inhibitors in combination with romidepsin stabilized BIM_{EL} to promote apoptosis (Chakraborty *et al.* 2013). For romidepsin treated THJ-16T and THJ-29T cells, we showed that pErk was present and not blocked which may have led to BIM_{EL} degradation. Thus, divergent patterns of p21 and BIM_{EL} regulation were identified related to the class of HDACi used leading to differential proteasome activation. This study documented the novel phenomenon whereby silencing p21 or BIM_{EL} allows the other protein to be expressed thereby switching the activity of the two HDACi classes with RhoB being necessary for either cell fate to occur. The mechanism by which multifaceted RhoB differentially 'decided' to promote either the p21 (cytostasis) or BIM_{EL} (apoptosis) pathway between class I and II HDACi remains to be elucidated. For example, when p21 was exclusively present, it led to G1 arrest and repression of BIM_{EL} (Collins *et al.* 2005). With class II inhibitors, BIM_{EL} protein was expressed across all four cell lines regardless of cell line mutation suggesting that the mutation does not regulate proteasome activity. Silenced *p21* in romidepsin treated cells mimicked the 'pro-p21' degradation activity of class II inhibitors, thus allowing BIM_{EL} expression. While intriguing, it remained to be explained why BIM_{EL} repression allowed stabilization of p21 and vice versa, why p21 repression allowed BIM_{EL} stabilization. Interestingly, combinatorial synergy of class II/(I) HDACi was not dependent upon microtubule stabilization when combined with paclitaxel as previously reported (Catalano *et al.* 2007). Instead, our data indicated that activation of the BIM_{EL} pathway dictated synergy. Thus, inhibiting HDAC6 led to RhoB-mediated induction of BIM_{EL} which led to G2/M arrest and apoptosis. On the other hand, inhibiting HDAC1 led to RhoB-mediated induction of p21 which led to G1 cell cycle arrest. These divergent RhoB pathways can be flipped between the two dictated by BIM_{EL} and p21 protein expression. Therefore, p21 and BIM_{EL} not only dictated apoptosis vs cell cycle arrest, but also dictated combinatorial synergy. This is clinically relevant since targeting BIM_{EL} for combination therapy would be most beneficial in patients with ATC. Ionizing radiation (IR) or other DNA damaging agents had been previously shown to lead to the induction of BIM_{EL} in a RhoB-dependent manner (Srougi & Burrige 2011). Therefore, we and others believed therapies should revolve around inducing expression of BIM_{EL} in cancer (Akiyama *et al.* 2009). The expression of BIM_{EL} mediated by

upregulated RhoB in response to therapy may be a biomarker of antitumor synergy with cytotoxic therapy such as paclitaxel. With the advent of novel specific HDAC6 inhibitors, HDAC6 may be a preferred molecular target for combinatorial therapeutic antitumor synergy, as suggested by others (reviewed in Li *et al.* (2013)), especially in patients with ATC. To support this premise, belinostat had demonstrated *in vivo* antitumor activity against ATC tumors grown in athymic nude mice (Chan *et al.* 2013). As well, there was a single case report of successful treatment of ATC with a combination of oral valproic acid, chemotherapy consisting of cisplatin and doxorubicin, external and intra-operative radiation and surgery (Noguchi *et al.* 2009). In summary, this report was the first to describe regulation of RhoB by HDAC6 and that RhoB down-stream effectors differentially regulated cell fate and chemotherapeutic synergy. These discovered differences may provide therapeutic benefit.

Supplementary data

This is linked to the online version of the paper at <http://dx.doi.org/10.1530/ERC-14-0302>.

Declaration of interest

The authors declare that there is no conflict of interest that could be perceived as prejudicing the impartiality of the research reported.

Funding

This work was supported by the National Institute of Health and Medical Research (R01CA136665; J A Copland, R C Smallridge), the Florida Department of Health Bankhead-Coley Cancer Research Program (FL09B202; J A Copland, R C Smallridge), a generous gift from Alfred D and Audrey M Petersen (R C Smallridge), the Francis and Miranda Childress Foundation Fund for Cancer Research (J A Copland), John A and Bette B Klacsmann Fund for Cancer Research at Mayo Clinic in Florida (J A Copland), and the Betty G Castigliano Fund in Cancer Research Honoring S Gordon Castigliano, MD cancer research at Mayo Clinic Florida (J A Copland).

Author contribution statement

L A Marlow contributed to experimental conception and design, acquisition of data, interpretation of data, and writing/revision of manuscript. I Bok contributed to acquisition of data, interpretation of data and editing of manuscript. R C Smallridge contributed to experimental conception and design, editing of manuscript and providing funding. J A Copland contributed to experimental conception and design, editing/approval of manuscript and providing funding.

Acknowledgements

We thank Dr Jason Hall for editing this manuscript and Dr Antonio DiCristofano for helpful suggestions. We are greatly appreciative to

Drs James Fagin and Jeffrey Knaufl for mutational analysis of our four ATC cell lines.

References

- [no authors] 2015 Panobinostat approved for multiple myeloma. *Cancer Research* **5** OF4. (doi:10.1158/2159-8290.CD-NB2015-040)
- Ader I, Toulas C, Dalenc F, Delmas C, Bonnet J, Cohen-Jonathan E & Gilles Favre G 2002 RhoB controls the 24 kDa FGF-2-induced radioresistance in HeLa cells by preventing post-mitotic cell death. *Oncogene* **21** 5998–6006. (doi:10.1038/sj.onc.1205746)
- Adnane J, Muro-Cacho C, Mathews L, Sebti SM & Munoz-Antonia T 2002 Suppression of RhoB expression in invasive carcinoma from head and neck cancer patients. *Clinical Cancer Research* **8** 2225–2232.
- Agarwal B, Halmos B, Feoktistov AS, Protiva P, Ramey WG, Chen M, Pothoulakis C, Lamont JT & Holt PR 2002 Mechanism of lovastatin-induced apoptosis in intestinal epithelial cells. *Carcinogenesis* **23** 521–528. (doi:10.1093/carcin/23.3.521)
- Ahn J, Choi J-H, Won M, Kang C-M, Gyun M-R, Park H-M, Kim C-H & Chung K-S 2011 The activation of p38 MAPK primarily contributes to UV-induced RhoB expression by recruiting the c-Jun and p300 to the distal CCAAT box of the RhoB promoter. *Biochemical and Biophysical Research Communications* **409** 211–216. (doi:10.1016/j.bbrc.2011.04.121)
- Ain KB, Egorin MJ & DeSimone PA 2000 Treatment of anaplastic thyroid carcinoma with paclitaxel: phase 2 trial using ninety-six-hour infusion. Collaborative Anaplastic Thyroid Cancer Health Intervention Trials (CATCHIT) Group. *Thyroid* **10** 587–594. (doi:10.1089/thy.2000.10.587)
- Akiyama T, Dass CR & Choong PF 2009 Bim-targeted cancer therapy: a link between drug action and underlying molecular changes. *Molecular Cancer Therapeutics* **8** 3173–3180. (doi:10.1158/1535-7163.MCT-09-0685)
- Allal C, Pradines A, Hamilton AD, Sebti SM & Favre G 2002 Farnesylated RhoB prevents cell cycle arrest and actin cytoskeleton disruption caused by the geranylgeranyltransferase I inhibitor GGTI-298. *Cell Cycle* **1** 430–437. (doi:10.4161/cc.1.6.272)
- Altmann A, Markert A, Askoxylakis V, Schöning T, Jesenofsky R, Eisenhut M & Haberkorn U 2012 Antitumor effects of proteasome inhibition in anaplastic thyroid carcinoma. *Journal of Nuclear Medicine* **53** 1764–1771. (doi:10.2967/jnumed.111.101295)
- Bertos N, Wang A & Yang X 2001 Class II histone deacetylases: structure, function, and regulation. *Biochemistry and Cell Biology* **79** 243–252. (doi:10.1139/o01-032)
- Borbone E, Berlingieri MT, De Bellis F, Nebbioso A, Chiappetta G, Mai A, Altucci L & Fusco A 2010 Histone deacetylase inhibitors induce thyroid cancer-specific apoptosis through proteasome-dependent inhibition of TRAIL degradation. *Oncogene* **29** 105–116. (doi:10.1038/onc.2009.306)
- Boyault C, Gilquin B, Zhang Y, Rybin V, Garman E, Meyer-Klaucke W, Matthias P, Muller CW & Khochbin S 2006 HDAC6-p97/VCP controlled polyubiquitin chain turnover. *EMBO Journal* **25** 3357–3366. (doi:10.1038/sj.emboj.7601210)
- Boyault C, Sadoul K, Pabion M & Khochbin S 2007 HDAC6, at the crossroads between cytoskeleton and cell signaling by acetylation and ubiquitination. *Oncogene* **26** 5468–5476. (doi:10.1038/sj.onc.1210614)
- Catalano MG, Poli R, Pugliese M, Fortunati N & Bocuzzi G 2007 Valproic acid enhances tubulin acetylation and apoptotic activity of paclitaxel on anaplastic thyroid cancer cell lines. *Endocrine-Related Cancer* **14** 839–845. (doi:10.1677/ERC-07-0096)
- Chakraborty AR, Robey RW, Luchenko VL, Zhan Z, Piekarsz RL, Gillet JP, Kossenkov AV, Wilkerson J, Showe LC, Gottesman MM et al. 2013 MAPK pathway activation leads to Bim loss and histone deacetylase inhibitor resistance: rationale to combine romidepsin with an MEK inhibitor. *Blood* **121** 4115–4125. (doi:10.1182/blood-2012-08-449140)
- Chan D, Zheng Y, Tyner J, Chng W, Chien W, Gery S, Leong G, Braunstein G & Koeffler HP 2013 Belinostat and panobinostat (HDACi): *in vitro* and *in vivo* studies in thyroid cancer. *Journal of Cancer Research and Clinical Oncology* **139** 1507–1514. (doi:10.1007/s00432-013-1465-6)
- Chen Y-X, Li Z-B, Diao F, Cao D-M, Fu C-C & Lu J 2006 Up-regulation of RhoB by glucocorticoids and its effects on the cell proliferation and NF- κ B transcriptional activity. *Journal of Steroid Biochemistry and Molecular Biology* **101** 179–187. (doi:10.1016/j.jsbmb.2006.06.030)
- Chou TC & Talalay P 1984 Quantitative analysis of dose-effect relationships: the combined effects of multiple drugs or enzyme inhibitors. *Advances in Enzyme Regulation* **22** 27–55. (doi:10.1016/0065-2571(84)90007-4)
- Collins NL, Reginato MJ, Paulus JK, Sgroi DC, LaBaer J & Brugge JS 2005 G1/S cell cycle arrest provides anoikis resistance through Erk-mediated Bim suppression. *Molecular and Cellular Biology* **25** 5282–5291. (doi:10.1128/MCB.25.12.5282-5291.2005)
- Copland JA, Marlow LA, Kurakata S, Fujiwara K, Wong AK, Kreinest PA, Williams SF, Haugen BR, Klopper JP & Smallridge RC 2006 Novel high-affinity PPAR γ agonist alone and in combination with paclitaxel inhibits human anaplastic thyroid carcinoma tumor growth via p21WAF1/CIP1. *Oncogene* **25** 2304–2317. (doi:10.1038/sj.onc.1209267)
- Delarue FL, Adnane J, Joshi B, Blaskovich MA, Wang DA, Hawker J, Bizouarn F, Ohkanda J, Zhu K, Hamilton AD et al. 2007 Farnesyltransferase and geranylgeranyltransferase I inhibitors upregulate RhoB expression by HDAC1 dissociation, HAT association and histone acetylation of the RhoB promoter. *Oncogene* **26** 633–640. (doi:10.1038/sj.onc.1209819)
- Du W & Prendergast GC 1999 Geranylgeranylated RhoB mediates suppression of human tumor cell growth by farnesyltransferase inhibitors. *Cancer Research* **59** 5492–5496.
- Fritz G & Kaina B 2001 Transcriptional activation of the small GTPase gene rhoB by genotoxic stress is regulated via a CCAAT element. *Nucleic Acids Research* **29** 792–798. (doi:10.1093/nar/29.3.792)
- Furumai R, Matsuyama A, Kobashi N, Lee KH, Nishiyama M, Nakajima H, Tanaka A, Komatsu Y, Nishino N, Yoshida M et al. 2002 FK228 (depsipeptide) as a natural prodrug that inhibits class I histone deacetylases. *Cancer Research* **62** 4916–4921.
- Gao L, Cueto MA, Asselbergs F & Atadja P 2002 Cloning and functional characterization of HDAC11, a novel member of the human histone deacetylase family. *Journal of Biological Chemistry* **277** 25748–25755. (doi:10.1074/jbc.M111871200)
- Ishida H, Zhang X, Erickson K & Ray P 2004 Botulinum toxin type A targets RhoB to inhibit lysophosphatidic acid-stimulated actin reorganization and acetylcholine release in nerve growth factor-treated PC12 cells. *Journal of Pharmacology and Experimental Therapeutics* **310** 881–889. (doi:10.1124/jpet.104.065318)
- Jiang K, Delarue FL & Sebti SM 2003 EGFR, ErbB2 and Ras but not Src suppress RhoB expression while ectopic expression of RhoB antagonizes oncogene-mediated transformation. *Oncogene* **23** 1136–1145. (doi:10.1038/sj.onc.1207236)
- Jiang K, Sun J, Cheng J, JY D, Wei S & Sebti S 2004 Akt mediates Ras downregulation of RhoB, a suppressor of transformation, invasion, and metastasis. *Molecular and Cellular Biology* **24** 5565–5576. (doi:10.1128/MCB.24.12.5565-5576.2004)
- Kaliszczak M, Trousil S, Aberg O, Perumal M, Nguyen QD & Aboagye EO 2013 A novel small molecule hydroxamate preferentially inhibits HDAC6 activity and tumour growth. *British Journal of Cancer* **108** 342–350. (doi:10.1038/bjc.2012.576)
- Khan N, Jeffers M, Kumar S, Hackett C, Boldog F, Khramtsov N, Qian X, Mills E, Berghs SC, Carey N et al. 2008 Determination of the class and isoform selectivity of small-molecule histone deacetylase inhibitors. *Biochemical Journal* **409** 581–589. (doi:10.1042/BJ20070779)
- Kim B-K, Im J-Y, Han G, Lee W-J, Won K-J, Chung K-S, Lee K, Ban HS, Song K & Won M 2014 p300 cooperates with c-Jun and PARP-1 at the p300 binding site to activate RhoB transcription in NSC126188-mediated apoptosis. *Biochimica et Biophysica Acta* **1839** 364–373. (doi:10.1016/j.bbagr.2014.03.004)

- Lee HZ, Kwitkowski VE, DelValle PL, Ricci MS, Saber H, Habtemariam BA, Bullock J, Bloomquist E, LiShen Y & Chen XH 2015 FDA approval: belinostat for the treatment of patients with relapsed or refractory peripheral T-cell lymphoma. *Clinical Cancer Research* **21** 2666–2670. (doi:10.1158/1078-0432.CCR-14-3119)
- Li Y, Shin D & Kwon SH 2013 Histone deacetylase 6 plays a role as a distinct regulator of diverse cellular processes. *FEBS Journal* **280** 775–793. (doi:10.1111/febs.12079)
- Li Y, Zhang X, Polakiewicz RD, Yao T-P & Comb MJ 2008 HDAC6 is required for epidermal growth factor-induced β -catenin nuclear localization. *Journal of Biological Chemistry* **283** 12686–12690. (doi:10.1074/jbc.C700185200)
- Mai A, Massa S, Pezzi R, Simeoni S, Rotili D, Nebbioso A, Scognamiglio A, Altucci L, Loidl P & Brosch G 2005 Class II (IIa)-selective histone deacetylase inhibitors. 1. Synthesis and biological evaluation of novel (aryloxopropenyl)pyrrolyl hydroxyamides. *Journal of Medicinal Chemistry* **48** 3344–3353. (doi:10.1021/jm049002a)
- Marlow LA, Reynolds LA, Cleland AS, Cooper SJ, Gumz ML, Kurakata S, Fujiwara K, Zhang Y, Sebo T, Grant C et al. 2009 Reactivation of suppressed RhoB is a critical step for the inhibition of anaplastic thyroid cancer growth. *Cancer Research* **69** 1536–1544. (doi:10.1158/0008-5472.CAN-08-3718)
- Marlow LA, D'Innocenzi J, Zhang Y, Rohl SD, Cooper SJ, Sebo T, Grant C, McIver B, Kasperbauer JL, Wadsworth JT et al. 2010 Detailed molecular fingerprinting of four new anaplastic thyroid carcinoma cell lines and their use for verification of RhoB as a molecular therapeutic target. *Journal of Clinical Endocrinology and Metabolism* **95** 5338–5347. (doi:10.1210/jc.2010-1421)
- Mazieres J, Antonia T, Daste G, Muro-Cacho C, Berchery D, Tillement V, Pradines A, Sebti S & Favre G 2004 Loss of RhoB expression in human lung cancer progression. *Clinical Cancer Research* **10** 2742–2750. (doi:10.1158/1078-0432.CCR-03-0149)
- Mazieres J, Tillement V, Allal C, Clanet C, Bobin L, Chen Z, Sebti SM, Favre G & Pradines A 2005 Geranylgeranylated, but not farnesylated, RhoB suppresses Ras transformation of NIH-3T3 cells. *Experimental Cell Research* **304** 354–364. (doi:10.1016/j.yexcr.2004.10.019)
- Mitsiades CS, Poulaki V, McMullan C, Negri J, Fanourakis G, Goudopoulou A, Richon VM, Marks PA & Mitsiades N 2005 Novel histone deacetylase inhibitors in the treatment of thyroid cancer. *Clinical Cancer Research* **11** 3958–3965. (doi:10.1158/1078-0432.CCR-03-0776)
- Nebbioso A, Manzo F, Miceli M, Conte M, Manente L, Baldi A, De Luca A, Rotili D, Valente S, Mai A et al. 2009 Selective class II HDAC inhibitors impair myogenesis by modulating the stability and activity of HDAC-MEF2 complexes. *EMBO Reports* **10** 776–782. (doi:10.1038/embor.2009.88)
- New M, Olzscha H & La Thangue NB 2012 HDAC inhibitor-based therapies: can we interpret the code? *Molecular Oncology* **6** 637–656. (doi:10.1016/j.molonc.2012.09.003)
- Noguchi H, Yamashita H, Murakami T, Hirai K, Noguchi Y, Maruta J, Yokoi T & Noguchi S 2009 Successful treatment of anaplastic thyroid carcinoma with a combination of oral valproic acid. Chemotherapy, radiation and surgery. *Endocrine Journal* **56** 245–249. (doi:10.1507/endocrj.K08E-016)
- Prendergast GC 2001a Actin' up: RhoB in cancer and apoptosis. *Nature Reviews. Cancer* **1** 162–168. (doi:10.1038/35101096)
- Prendergast G 2001b Farnesyltransferase inhibitors define a role for RhoB in controlling neoplastic pathophysiology. *Histology and Histopathology* **16** 269–275.
- Prince HM, Bishton MJ & Harrison SJ 2009 Clinical studies of histone deacetylase inhibitors. *Clinical Cancer Research* **15** 3958–3969. (doi:10.1158/1078-0432.CCR-08-2785)
- Ramesh S, Wildey GM & Howe PH 2009 Transforming growth factor β (TGF β)-induced apoptosis: the rise and fall of Bim. *Cell Cycle* **8** 11–17. (doi:10.4161/cc.8.1.7291)
- Sambucetti LC, Fischer DD, Zabludoff S, Kwon PO, Chamberlin H, Trogiani N, Xu H & Cohen D 1999 Histone deacetylase inhibition selectively alters the activity and expression of cell cycle proteins leading to specific chromatin acetylation and antiproliferative effects. *Journal of Biological Chemistry* **274** 34940–34947. (doi:10.1074/jbc.274.49.34940)
- Schmittgen TD & Livak KJ 2008 Analyzing real-time PCR data by the comparative C(T) method. *Nature Protocols* **3** 1101–1108. (doi:10.1038/nprot.2008.73)
- Smallridge RC, Marlow LA & Copland JA 2009 Anaplastic thyroid cancer: molecular pathogenesis and emerging therapies. *Endocrine-Related Cancer* **16** 17–44. (doi:10.1677/ERC-08-0154)
- Smallridge RC, Copland JA, Brose MS, Wadsworth JT, Houvras Y, Menefee ME, Bible KC, Shah MH, Gramza AW, Klopper JP et al. 2013 Efatutazone, an oral PPAR- γ agonist, in combination with paclitaxel in anaplastic thyroid cancer: results of a multicenter phase 1 trial. *Journal of Clinical Endocrinology and Metabolism* **98** 2392–2400. (doi:10.1210/jc.2013-1106)
- Srougi MC & Burridge K 2011 The nuclear guanine nucleotide exchange factors Ect2 and Net1 regulate RhoB-mediated cell death after DNA damage. *PLoS ONE* **6** e17108. (doi:10.1371/journal.pone.0017108)
- Vaziri H, Dessain SK, Eaton EN, Imai S-I, Frye RA, Pandita TK, Guarente L & Weinberg RA 2001 hSIR2/SIRT1 functions as an NAD-dependent p53 deacetylase. *Cell* **107** 149–159. (doi:10.1016/S0092-8674(01)00527-X)
- Vishnu P, Colon-Otero G, Kennedy GT, Marlow LA, Kennedy WP, Wu KJ, Santoso JT & Copland JA 2012 RhoB mediates antitumor synergy of combined ixabepilone and sunitinib in human ovarian serous cancer. *Gynecologic Oncology* **124** 589–597. (doi:10.1016/j.ygyno.2011.11.019)
- Wang S, Yan-Neale Y, Fischer D, Zeremski M, Cai R, Zhu J, Asselbergs F, Hampton G & Cohen D 2003 Histone deacetylase 1 represses the small GTPase RhoB expression in human non-small lung carcinoma cell line. *Oncogene* **22** 6204–6213. (doi:10.1038/sj.onc.1206653)
- Wang S, Yan-Neale Y, Zeremski M & Cohen D 2004 Transcription regulation by histone deacetylases. *Novartis Foundation Symposium* **259** 238–245.
- Zhao Y, Tan J, Zhuang L, Jiang X, Liu ET & Yu Q 2005 Inhibitors of histone deacetylases target the Rb-E2F1 pathway for apoptosis induction through activation of proapoptotic protein Bim. *PNAS* **102** 16090–16095. (doi:10.1073/pnas.0505585102)
- Zhou X, Marks PA, Rifkind RA & Richon VM 2001 Cloning and characterization of a histone deacetylase, HDAC9. *PNAS* **98** 10572–10577. (doi:10.1073/pnas.191375098)

Received in final form 16 July 2015

Accepted 23 July 2015

Made available online as an Accepted Preprint

23 July 2015